SATURABLE CORE REACTORS

Saturable core reactors are inductors with core materials the magnetic flux of which saturates when the exciting current of the coil exceeds a certain level, and the saturation is positively utilized to obtain special features in addition to a nonsaturable ordinal inductor's (reactor's) features.

In general, magnetic saturation is recognized as an undesirable feature of magnetic core materials because the saturation often limits the highest applicable voltage and current, or limits the capability of power and quality provided in electrical apparatus. Saturation, however, adds excellent features to machines when it exists with magnetic reactors; that is, suppressing undesirable oscillations of the system, increasing system stability, protecting circuit devices, etc., are their typical usages. In this article the basic principles of saturable core reactors are explained, and then their applications, the properties and the appropriate selection of materials, and the basic designing method of the core are stated.

BASIC CHARACTERISTICS

Figure 1 introduces a basic idea of magnetic flux and magnetizing current. Magnetic flux ϕ in the core is established by energizing the copper coil by magnetizing current i. Assuming the turn number of the coil is n, the relationship between ϕ (Wb) and i (A) is described by Faraday law:

$$e = n\frac{d\phi}{dt} = \frac{d\lambda}{dt}(\lambda = n\phi) \tag{1}$$

where e is the induced voltage of the coil, and $\lambda = n\phi$ is called the *magnetic flux linkage* or simply *flux linkage*. This equation can also be written in the form

$$e = \frac{d\lambda}{dt} = \frac{d\lambda}{di}\frac{di}{dt} \tag{2}$$

If using the inductance L(H) of the coil, setting

$$\frac{d\lambda}{di} = L \tag{3}$$

we obtain

$$e = L\frac{di}{dt} \tag{4}$$

In the preceding equation, when the core material is not saturated, the inductance L has a constant value. While a saturable core is used in the coil, the core saturates according to an increase of magnetizing current i, then the flux/or flux linkage (λ) in the core shows a saturated characteristic as depicted in Fig. 3. The characteristic curve is only an approximate expression, although the actual characteristics are extremely complex with complicated hysteresis, and the complexity depends on temperature, pressure, and/or other surrounding materials.

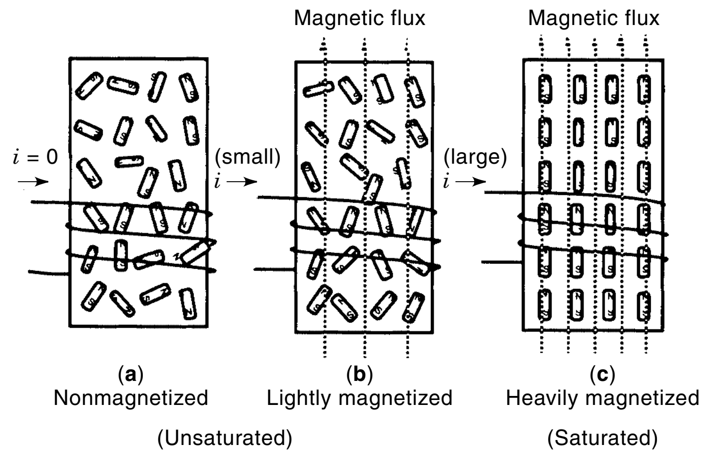

Figure 2. Magnetizing characteristics and the definition of saturation threshold.

The saturation characteristics are simply approximated for industrial use by the two folded lines drawn in Fig. 3. In this approximation the saturation occurs over $+\Lambda_s$ or below $-\Lambda_s$. The symbols expressing the saturable reactor cores are also placed in Fig. 3. Nevertheless the complexity, the saturated characteristic of Fig. 3 is given a simple and clear comprehensive explanation by the alignment of magnetic domains in Fig. 2. The domain, although this is only an assumption, is the smallest unit of magnetism that shows north and south poles.

Looking at the polarization of the core with magnetizing coil in Fig. 2, case (a) of no magnetization shows that the domains are randomly polarized; consequently the total north and south poles are never seen from the outside of the core. Figure 2(b), with slight magnetization, shows a slightly oriented condition and north polarity in the up direction. In Fig. 2(c), the heavily magnetized case, all domains are completely aligned to the direction of the applied magnetic field produced by exciting i. The increase of the total flux after complete saturation will be only from the permeability of the air or vacuum depending on the surroundings.

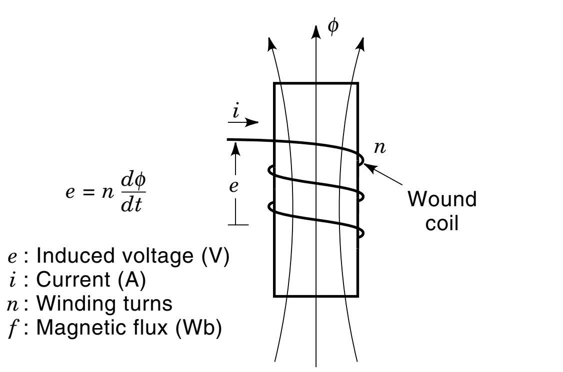

Figure 1. Magnetic flux and induced voltage (Faraday's law).

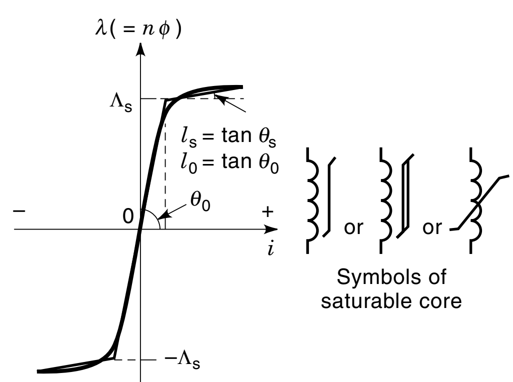

Figure 3. Magnetizing process.

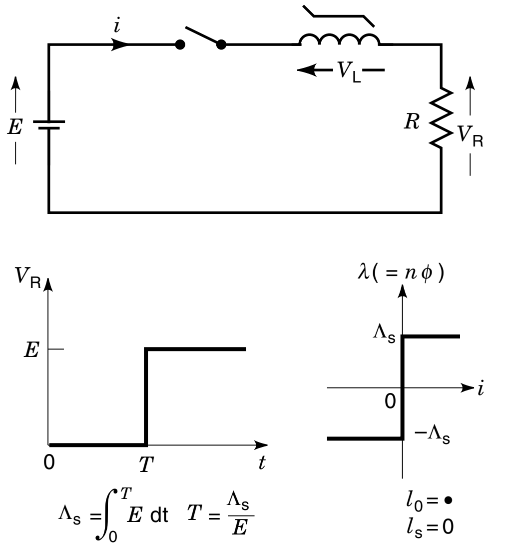

Figure 4. Delay switch.

The two folded lines of Fig. 3 mean that $d\lambda/di$ has two values depending on the situation, that is, saturated or not; the inductances are assigned to l in the linear nonsaturated region and l_s in satured region. On the other hand, the definition

$$\lambda = n\phi = Li \tag{5}$$

is often adopted for electric and electronic areas. This is not valid in the exact sense of Eq. (3).

TIME DELAY CIRCUIT

A typical and interesting usage of the saturable reactor is the delay circuit in Fig. 4. The source voltage E is applied to resistor load R, and a saturable reactor is inserted in series to R. With the assumption that the saturable core has the characteristic depicted in Fig. 4, the core shows extremely high (infinitive) inductance for nonsaturated region, while it shows very low inductance l_s (=0) in the saturated region.

The flux linkage λ of the core varies as Eq. (1); hence, the voltage across the core is

$$v_L = \frac{d\lambda}{dt} \tag{6}$$

Rewriting it into integral form gives

$$\lambda = \int_0^t v_L\,dt \tag{7}$$

When switch S is turned on at $t = 0$, current i does not flow immediately because of infinite inductance. Then $v_L = E$ and Eq. (7) becomes

$$\lambda = \int_0^t E\,dt = Et \tag{8}$$

When λ reaches Λ_s at $t = T$, the core saturates and shows very low inductance ($l_s = 0$). By setting $\lambda = \Lambda_s$ in Eq. (6),

$$v_L = 0 \tag{9}$$

Then the current i suddenly begins to flow, just as if E is applied across resistor R. The delay time T can be obtained by substituting $t = T$ and in Eq. (8):

$$T = \frac{\Lambda_s}{E} \tag{10}$$

CURRENT LIMITERS

The current limiter is one of the major applications of saturable reactor cores. In Fig. 5, a semiconductor switch S is placed to feed voltage E upon a load. Two examples of current and voltage of the turning-on switch are depicted. In Fig. 5(a), the resultant current-rise region (dotted line) and the corresponding voltage-fall region (solid line) overlap and the switching loss p_{loss} occurs, as noted in the figure. If the saturable reactor is placed between source E and the load, the current i will be delayed by T. The switching loss can then be extremely reduced.

Figure 5(b) shows reduction of the rush current. The oscillatory rush current (dashed line) often arises due to stray capacitance and stray inductance around the load. This current peak damages the device itself or the insulation of the load. The saturable reactor is effectively used to remove this kind of rush current, although an additional snubbing circuit may be necessary around the switch S.

SIMILARITY TO THE SILICON-CONTROLLED RECTIFIER IN AC VOLTAGE CONTROL (1)

A typical switching device, [the silicon-controlled rectifier (SCR) or thyristor] is used to switch the load in and out from

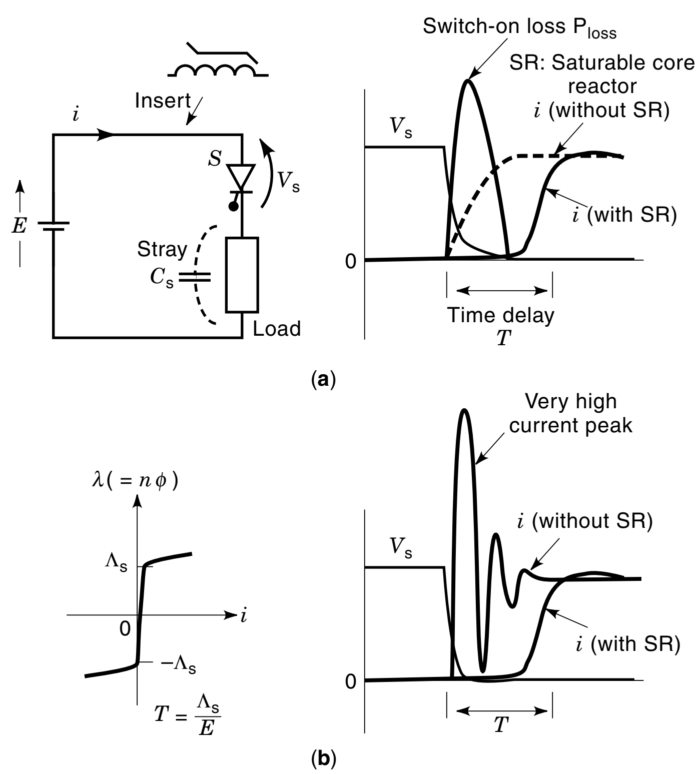

Figure 5. Application with semiconductor switching devices (avoiding switch-on rush current, reduction of switching losses, etc.).

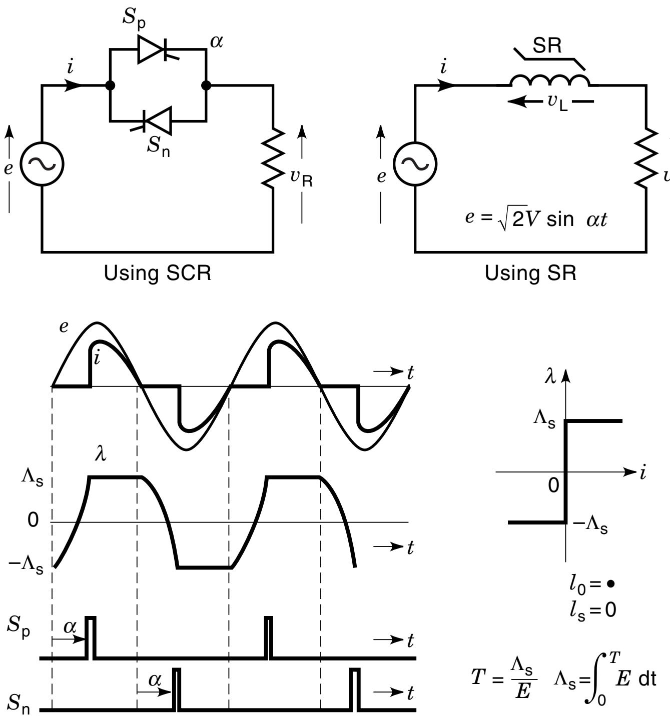

Figure 6. Duality with SCR in ac phase control.

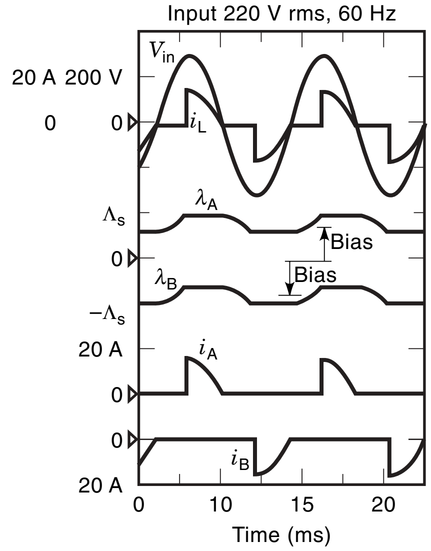

Figure 8. Waveforms of the magnetic amplifier.

the power source e as shown in Fig. 6. The action is quite similar to that of a saturable core reactor circuit depicted in the same figure. Exactly the same waveforms of voltage v_R and current i are obtained for these two cases. The waveforms of flux linkage λ of the saturable core and the corresponding gating pulses of SCR are also depicted in the figure. The saturated region obviously corresponds to the conducting period of SCR.

MAGNETIC AMPLIFIERS (2)

The firing angle α in Fig. 6 is usually varied by electronic circuit for SCR circuit, whereas the Λ_s or winding turn n cannot be changed for the saturable core reactor (SR). The technique to vary α in a staturable core can be realized by adding bias current to the coil. The typical implementation with this technique is called as magnetic amplifier (MA). Many kinds of MA circuits have been proposed in the past and have been used for practical ac voltage control, enabling motor speed control, heat control, lighting control, and so on. Figure 7 is one of the popular MA circuits. It has two saturable core reactors (SR_A, SR_B) with a control winding that adds dc biasing to each core. The resulting waveforms are shown in Fig. 8, and the biasing current displaces λ_A upward, λ_B down, so that SR_A conducts to flow i_A in the positive direction; alternately SR_B conducts to flow i_B in negative direction. The resulting load current i_L has a phase-controlled ac current just the same as in Fig. 6. If the control current I_c is changed, the biasing level changes, then the control angle α changes. The control current I_c is normally fed through a large inductance and resistor connected in series to an additional dc voltage source. Normally the control winding has far more turns than the main winding has, so that current I_c is very small compared to the main current level. Even if a dc voltage source with a series resistor is used to feed I_c, the high inductance of the control winding easily filters the current ripple away. At that time, the losses in the resistor become quite small due to small I_c.

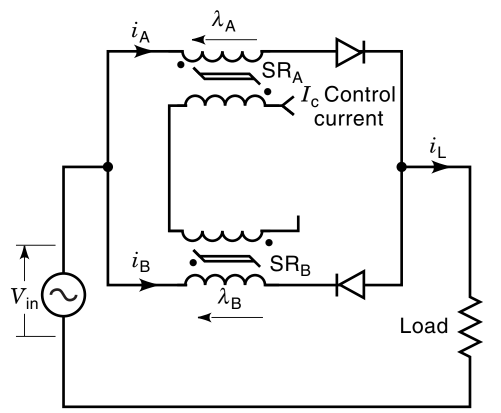

Figure 7. Parallel connection magnetic amplifier.

CURRENT-PULSE-PEAK LIMITING (3)

Another interesting example of a saturable core reactor is current-pulse-peak limiting as shown in Figs. 9 and 10. In Fig. 9(a), if the switch S (SCR) is not fired, the current source feeds current I_d to capacitor C_0, and the voltage v_{c0} increases to the polarity of right side positive. When the voltage v_s, across switch S exceeds a certain preset level (500 V for this case), a gating pulse is fed to the gate of the SCR. (This gating is done by an additional electronic circuit.) Current I_s starts flowing in a resonant way through C_0 and L_0 to the capacitor-input load, as shown in Fig. 9(b). When I_s reaches zero again, the SCR turns off. As the voltage v_{c0} becomes negative again, the charging by the current source I_d restarts. After a while, the voltage v_{c0} reaches the same preset value as before, then the SCR is fired, again and the next pulse appears.

These pulses have sinusoidal variations and the peak value becomes sometimes higher beyond the permissible level. To reduce this peak, the next current-pulse-peak limiting with a saturable core is a simple and reliable solution.

In Fig.10(a), a saturable reactor with a secondary winding ($1 : n$ = primary turns : secondary turns) is inserted at the con-

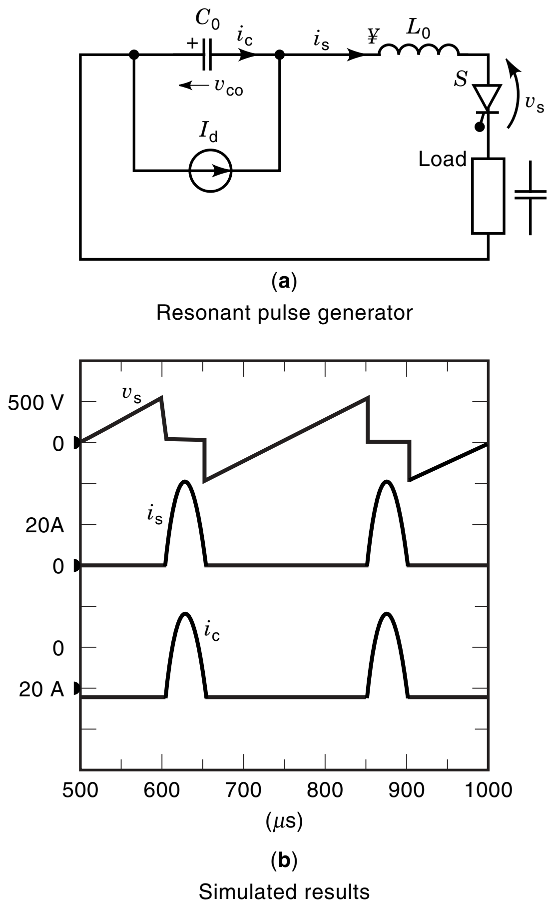

Figure 9. A current-pulse generator without saturable reactor. (a) Resonant pulse generator. (b) Simulated results.

necting point of current source I_d. For instance, the case $n = 3$ is calculated in the figure. The switching device S is gated at the threshold of $v_s = 500$ V as equal as that of previous one. The current I_s is limited by the level of 20 A for this case.

The limiting process is explained in Fig. 10(b). Assuming the saturable core has the I–λ characteristics as indicated in the figure for the primary coil only, the total magnetizing current I resulting from the two coils becomes

$$I = I_s - nI_d \tag{11}$$

where I_s is main winding current and I_d is the secondary coil current.

When the voltage v_s reaches 500 V, the SCR is gated and I_s starts to flow. This point is denoted as 1 in the figure. As the saturable core is in the saturated region the remaining inductance is very small, so that I_s increases almost as quickly as shown in Fig. 9. When reaching the saturable region, denoted as 2, the magnetizing current I becomes 0 (i.e., $I_s = nI_d$), and the equivalent inductance of SR suddenly jumps to an extremely high value (almost infinity in this figure). Although the flux changes toward region 3 in the figure, the condition $I = 0$ is maintained; hence $I_s = nI_d$ is ensured. After a while, both of the voltages across C_0 and SR reverse to their opposite polarities, and the flux linkage λ also begins to return back to 2, and then through the saturated region again, arriving at starting point 1.

In Fig. 11, an example of practical usage of this circuit is provided. This circuit is the so-called current-type resonant converter circuit, which converts ac commercial frequency power to the different frequency and different voltage three-phase ac output. The saturable core pulse generator is placed in the middle, and the current source is replaced by a large

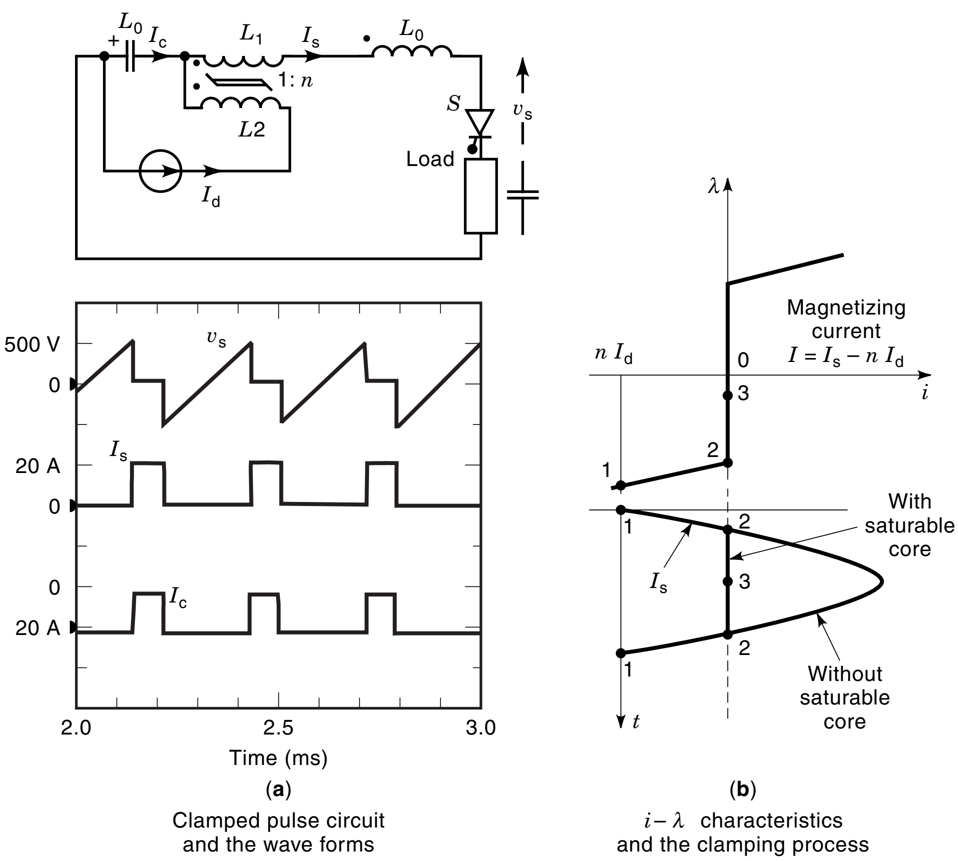

Figure 10. Current-peak limiting with a saturable reactor. (a) Clamped pulse circuit and waveforms. (b) I–λ characteristics and the clamping process.

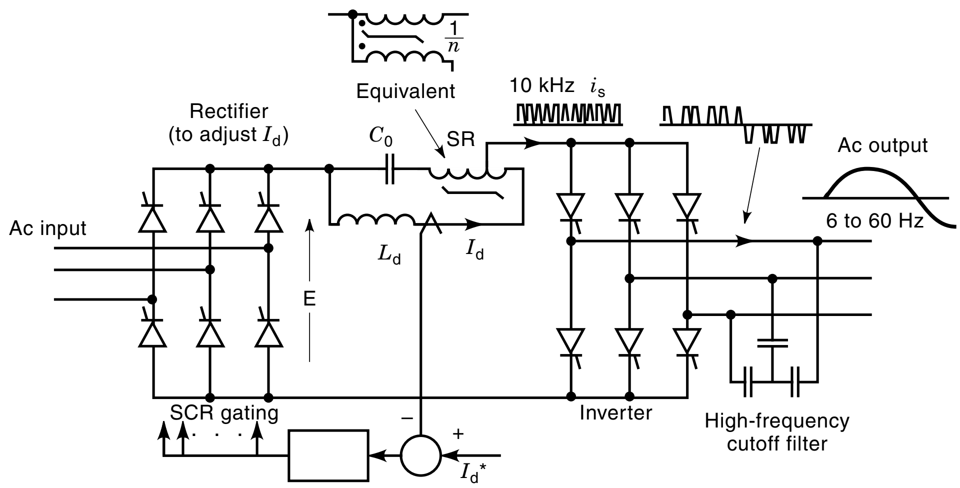

Figure 11. Resonant-converter application of current-pulse peak-limiting.

inductance L_d with current feedback. The detected I_d is compared to the reference value I_d^*, and the rectifier SCRs are gated to make I_d equal to I_d^*. The high-frequency pulses made from this clamped pulse circuit are distributed to obtain the required low-frequency output voltages, as depicted in the figure. As a high-frequency cutoff filter is placed between the output terminals, the three-phase ac output voltages or currents are relatively smooth.

SIMULATION WITH SATURABLE CORE REACTORS

Simulation of the circuit to obtain the circuit currents and voltages that already appeared in previous figure is normally performed by the process shown in Fig. 12. The process may be coded by Fortran, Basic, Pascal, C, etc. The most convenient method may be using SPICE-type simulation tools (4). In that case, at first, we prepare a net list to teach circuit configurations to the simulator, which can be easily done by using computer-aided design (CAD) input program, if available. The simulation begins by reading circuit configurations from the net list, and then preprocessing with the initial conditions is performed, as shown in the flow chart. The actual calculation proceeds by a time-step basis (the unit time step is ΔT), beginning from t (time) = 0. For each instant, the circuit simulator reads the actual inductance(s) or $d\lambda/di$ of the saturable core(s) corresponding to the dynamically changing current(s) of the saturable core(s). The new inductance value of the saturable core is used to replace old one. This replacement is essential to solve the circuit including a saturable core, just as including other nonlinear parts in the circuit.

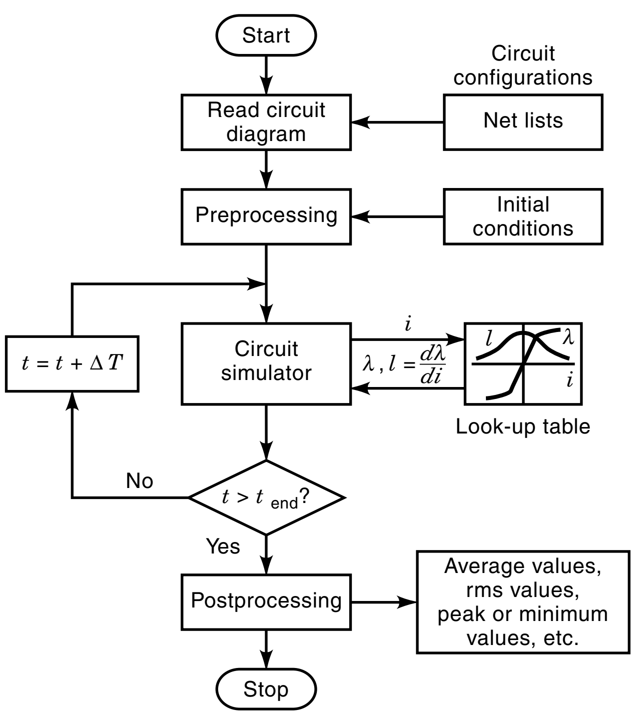

Figure 12. Simulating the process with a saturable core.

DESCRIBING-FUNCTION ANALYSIS (1,5)

The describing-function (DF) analysis of nonlinear elements is basically a fundamental component analysis. It is quite convenient to solve the circuit and to see the nature of the fundamental current and voltage, although the instantaneous wave shape is different from the previous time-step basis simulation. However, the DF analysis has the feature of using a simple function of nonlinear elements such as saturable reactor cores, and the use of a transfer function to solve system stability is quite convenient. Usually the system stability analysis needs many transfer functions for each element or each block. An example of the describing-function analysis is shown in Figs. 13 and 14. In Fig. 13, ac voltage is applied to the load resistor R, and a saturable reactor core is placed to adjust the current i. The waveforms of v_{in} and i are shown in the same figure. If observing the voltage v_L across the reactor, the waveshape becomes quite distorted, whereas the integrated value, that is, the magnetic flux linkage λ, shows quite a sinusoidal variation. If we assume this λ to be a sinusoidal wave, we obtain the current i' in Fig. 14. This waveshape is part of sinusoid; hence the fundamental component i_1 is expressed as a mathematical transfer function.

The resulting form $D(\beta)$ (describing function) of the saturable core is as follows:

$$D(\beta) = \frac{I_1}{\Lambda_1} = \frac{1}{\pi l_s}(\beta - \sin\beta) \tag{12}$$

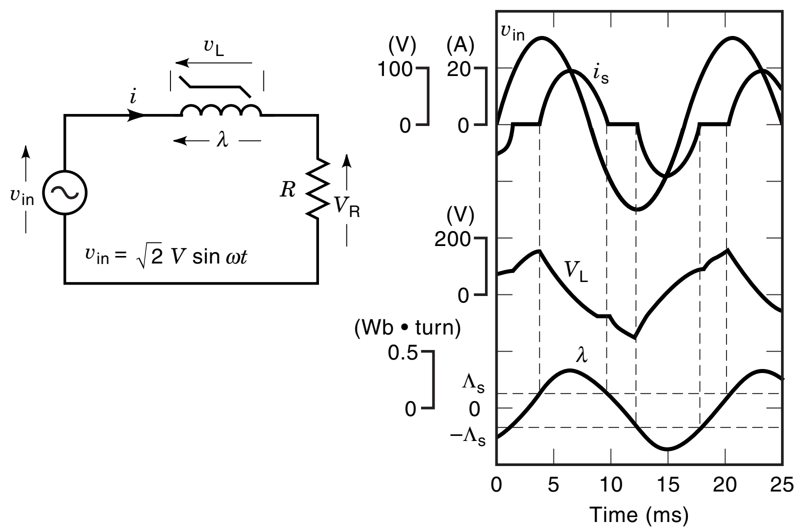

Figure 13. Describing-function analysis.

where β is a conduction angle of the saturable core, noted in the figure. If $D(\beta)$ is reciprocated, $1/D(\beta)$ becomes the equivalent inductance of the saturable core. In steady-state fundamental component analysis, the circuit in Fig. 13 reduces to a simple circuit, illustrated in Fig. 14. The current I_1 is obtainable from the common ac circuit calculation as shown in Eqs. (13) and (14). Kirchhoff's equation of the circuit is

$$\dot{V} = [R + j\omega l_s D(\beta)]\dot{I}_1 \tag{13}$$

Hence, the fundamental current $\dot{I}_1$ is obtained simply as

$$\dot{I}_1 = \dot{V}/[R + j\omega l_s D(\beta)]$$

or in rms value,

$$I_{1(\mathrm{rms})} = \dot{V}/\sqrt{R^2 + [\omega l_s D(\beta)]^2} \tag{14}$$

MAGNETIC PROPERTIES

The properties of magnetic materials are especially important for saturable cores to achieve the full operating performance. The high-frequency minor-loop losses and eddy-current losses not only deteriorate the efficiency, but also cause the temperature rise, and make the saturation unstable, resulting in system failure. Hereafter the nature and the properties of the saturable core materials appropriate for saturable core reactors are stated. Magnetic properties of materials required to saturable cores are as follows:

1. High permeability
2. Low coercive force
3. Low core loss
4. High saturation flux density

In general, the shape of a rectangular hysteresis loop (high squareness of the B–H loop) is needed, so that the B_r/B_s value of a magnetic material, which is called the squareness ratio, should be considerably high at any operating frequency. B_r is the remanence or residual flux density and B_s is the saturation flux density of the material, which is often replaced as B_{1000}, for example (meaning B at 1000 A/m) from a practical point of view. Here, B_r/B_s is used to describe the squareness ratio although B is not measured at saturation but at some magnetizing forces. Low B_r/B_s values cause a dead angle (uncontrollable time) and deteriorate automatic voltage regula-

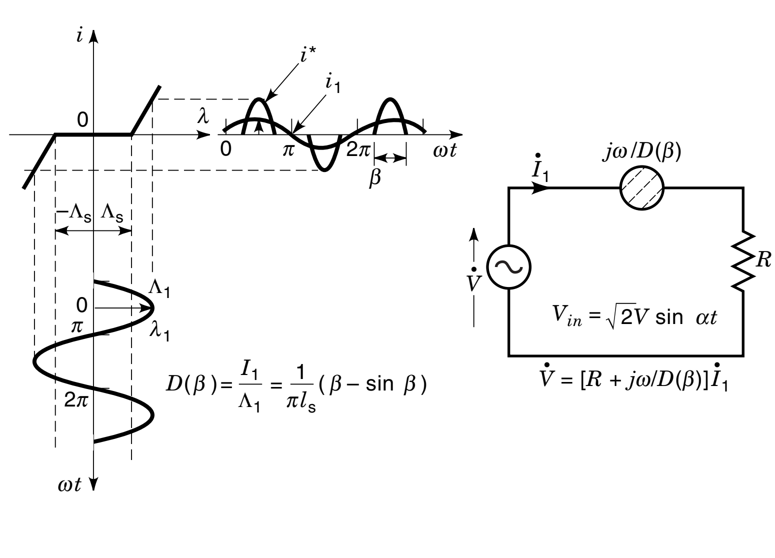

Figure 14. Equivalent circuit using the describing-function model.

tion ability. A large coercive force enlarges the exciting current and core loss, which raises the core temperature.

CORE MATERIALS

Magnetic materials that satisfy the preceding magnetic properties are

1. Grain-oriented silicon steel
2. 80 Ni–Fe permalloy
3. 50 Ni–Fe permalloy
4. Mn–Zn ferrite
5. Co-based amorphous alloy
6. Fe-based amorphous alloy
7. Nanocrystalline material (FINEMET by Hitachi Metal Industries)

Taking B_r/B_s into consideration for saturable cores, traditional magnetic anisotropic materials of grain-oriented 3% silicon steel and 50% Ni–Fe anisotropic (oriented) permalloy are available for low-frequency use, which have a relatively high B_s of 2.03 T and 1.6 T, respectively.

For saturable cores used in magnetic-amplifier-type power supplies, amorphous materials have been commonly used for application in power supplies operating at higher frequencies 200 kHz to 500 kHz, while the traditional 50% Ni–Fe anisotropic permalloy has been limited to below 50 kHz. Mn–Zn ferrite, the most representative of the high-permeability ferrites, is applicable to magnetic cores at frequencies of 10 kHz to 100 kHz but has low B_r/B_s.

Hysteresis curves are shown in Fig. 15 for grain-oriented silicon steel (3% Si–Fe), 50% Ni–Fe permalloy (50 Ni Fe), and 80% Ni–Fe permalloy (PCS), and in Fig. 16 for Co-based amorphous ribbon (CoAM) and Fe-based amorphous ribbon (FeAM) with PCS as a reference.

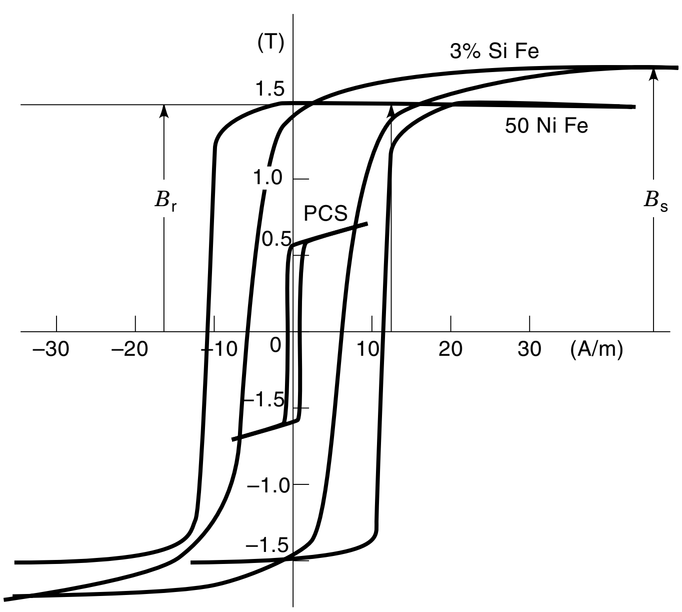

Figure 15. Hysteresis curves of 0.23 mm thick 3% Si highly grain-oriented steel, 0.1 mm thick anisotropic 50NiFe, and 0.1 mm thick PCS (78Ni5MoFe) materials.

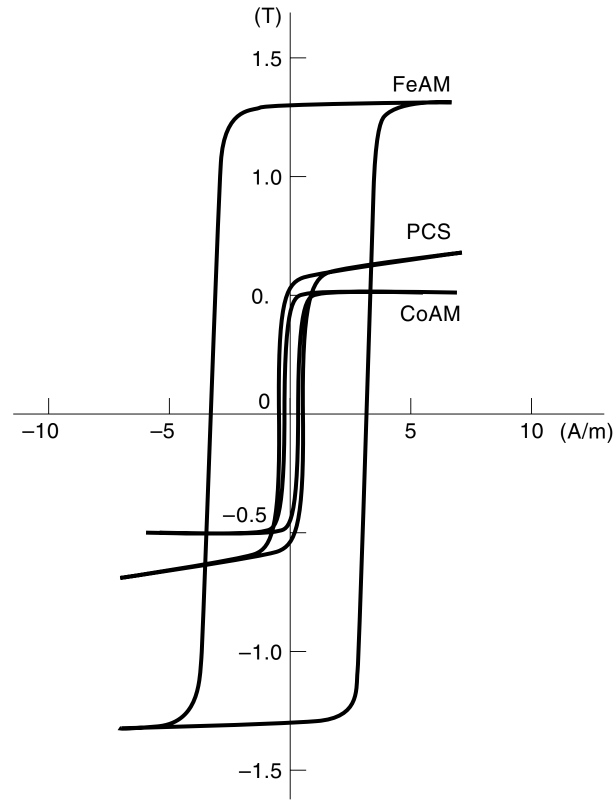

Figure 16. Hysteresis curves of Co-based amorphous (CoAM), Fe-based amorphous (FeAM) and PCS (78Ni5MoFe) materials.

Permalloy

50% Ni–Fe anisotropic (oriented) permalloy has a crystallization texture of (100)[100], Miller induces, produced by high-reduction cold-rolling and appropriate heat treatment, which exhibits high permeability and a rectangular hysteresis loop. Because of the high iron content of 50% the permalloy has the advantage of a higher saturation induction of B_s = 1.5 T to 1.6 T as well as a high initial permeability compared with 80 Ni–Fe permalloy (PCS). The remanence B_r is 1.4 T to 1.5 T and the coercivity is 2 A/m to 12 A/m. So, B_r/B_s is 92% to 99%. The maximum dc permeability is 80,000 to 200,000.

50% Ni–Fe permalloy is available as cold-rolled strip or tape of thickness is 0.1 mm to 0.01 mm. The cores should be protected from applied stress because magnetic properties of cores deteriorate easily due to strain applied during handling and winding (6).

Amorphous Material

Co-based amorphous (CoFe–Si–B) alloy has been very common for saturable cores in switching power supplies. Low coercivity and high permeability result from the absence of magnetocrystalline anisotropy, grain boundaries and secondary phases. Co-based amorphous alloys exhibit remarkably high permeability and low coercivity that originate from the zero-magnetostrictive nature, being obtained by controlling alloy composition with the addition of several percent of Fe, like $Co_{70}Fe_5Si_{15}B_{10}$ (atomic percent), for example. High electric resistivity and thinness of the ribbon rapidly quenched from the melt give the amorphous core extremely low loss in higher-frequency use above 100 kHz.

Fe-based amorphous materials, Fe–Ni–Si–B, for example, have higher B_s and B_r/B_s characteristics but larger coercivity or core loss at higher frequencies than Co-based amorphous cores as shown in Table 1. In the table, typical properties of coercive force, H_c, and B_r/B_s (B_{1000} is substituted for B_s) are shown for Co-based and Fe-based amorphous materials compared with traditional isotropic 50% Ni–Fe permalloy. Amorphous materials are available either as rapidly quenched ribbons or toroidal cores annealed for saturable cores. The ribbon thickness is around 20 mm with a high resistivity of 1.3 $\mu\Omega \cdot$ m to 1.5 $\mu\Omega \cdot$ m (7).

Ferrite

Soft ferrite materials with high initial permeability are Mn–Zn ferrite, Cu–Mn ferrite, and Mn–Mg ferrite. Mn–Zn ferrite has high permeability and low coercivity at high frequencies up to 1 MHz, but as for B_r/B_s, Mn–Zn ferrite is inferior to the amorphous or permalloy materials.

TEMPERATURE-DEPENDENT PROPERTIES

When a core is magnetized at high frequencies, the core temperature rises by eddy-current loss and affects the magnetic properties of the core. If a decrease of B_r/B_s and an increase of H_c of the core material by temperature rise become remarkably large, the characteristics of the saturable reactor core would deteriorate.

In general, the saturation magnetization B_s decreases with temperature so that the change of B_r/B_s would be small. In Figs. 17 and 18, the temperature-dependent B_r/B_s and H_c of the 50 Ni–Fe permalloy at 400 Hz and Co-based amorphous material at 50 kHz are shown, respectively. B_r/B_s decreases slightly in the permalloy and does not change in the Co-based amorphous core against temperature rise, while each H_c decreases in both cores. These tendencies suggest no increase of core loss during operation so that the same controlling conditions at room temperature are expected for these materials under the operating conditions (8,9).

MAGNETIZATION CHARACTERISTICS OF CORE MATERIALS

In saturable reactor cores, the magnetic material is magnetized from a working point to magnetic saturation of the hysteresis loop. In order to evaluate magnetic materials for saturable reactor cores, a measurement method to simulate saturable cores is proposed. The constant-current flux-reset (CCFR) method or the controlled-magnetization characteristics (CMC) method can imitate magnetizing conditions of a magnetic amplifier (10). Both reset and saturation characteristics can be measured with a simple circuit [Fig. 19(a)]. The reset characteristic is the field strength H, as shown in Fig. 19(b), required to reach the working point. The reset field strength and core loss become less, as the curve becomes steeper and closer to the vertical axis. Another characteristic is the flux density swing from remanence into saturation, ΔB_b in Fig. 19(a), which corresponds to the dead angle. The less ΔB_b becomes, the better the controlling characteristics are.

Figure 20 shows the controlled magnetization curves at 50 kHz of Co-based amorphous core (CoAM), 50% Ni–Fe permalloy core (50NiFe) and Mn–Zn ferrite (ferrite). At 50 kHz both the Mn–Zn ferrite core and the anisotropic 50% Ni–Fe core are inferior to the Co-based amorphous core. Figure 21 shows the frequency-dependent controlled magnetization curves of a Co-based amorphous core at 50 kHz, 100 kHz, and 200 kHz.

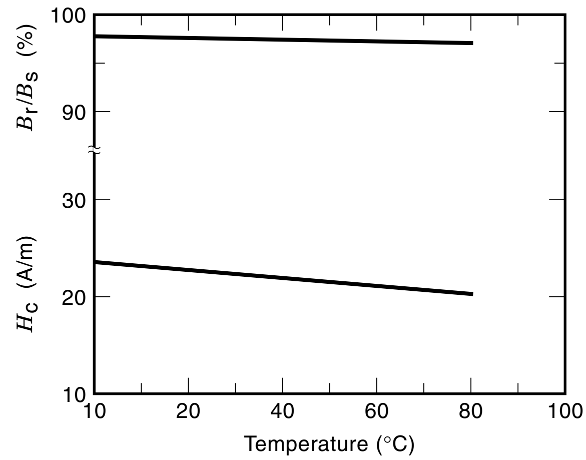

Figure 17. Temperature-dependent B_r/B_s and H_c of the 50% Ni–Fe permalloy (400 Hz, B_s = B160).

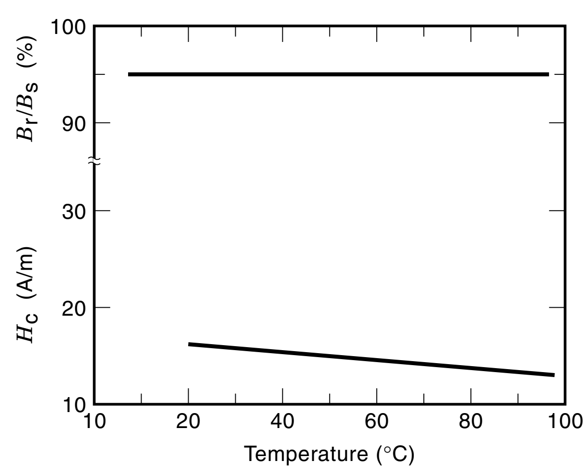

Figure 18. Temperature-dependent B_r/B_s and H_c of Co-based amorphous material (50 kHz).

Table 1. Typical Properties of H_c and B_r/B_s for Fe-Based, Co-Based Amorphous and 50 Ni–Fe Permalloy at the Frequencies of 20 kHz and 50 kHz

		20 kHz		50 kHz	
Material	Thickness (mm)	H_c (A/m)	B_r/B_1 (%)	H_c (A/m)	B_r/B_1 (%)
Fe-based amorphous	17	42	96	119	97
Co-based amorphous	14	5.6	91	10	98
50 Ni–Fe permalloy	25	73	98	—	—

B_1: B at 1000 A/m

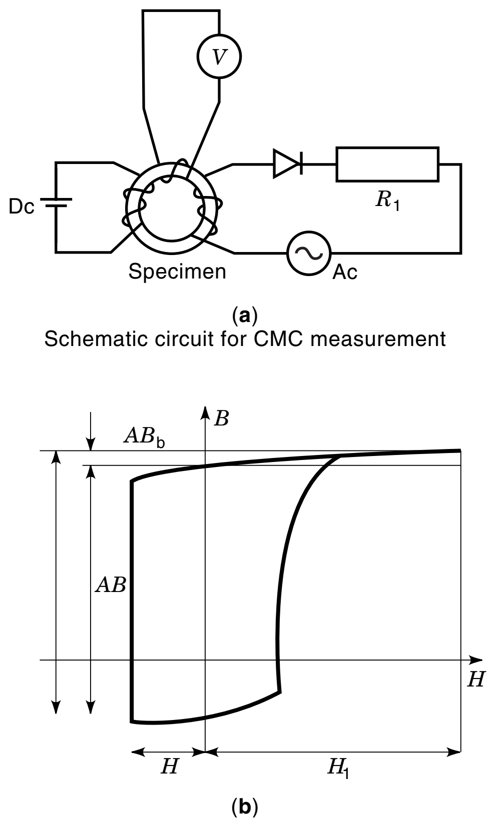

Figure 19. Controlled magnetization characteristic measurement. (a) Schematic circuit for CMC measurement. (b) Schematic *B*–*H* loop for CMC measurement.

DESIGNING SATURABLE CORES FOR MAGNETIC AMPLIFIER

The advantages of using magnetic amplifiers in switched-mode power supplies are

a. The design is simple with one core and one winding for load and regulation.
b. The reset is highly reliable.
c. The circuit is lined up straightforwardly.

A designing method for a forward converter with magnetic amplifier regulation is described briefly as follows:

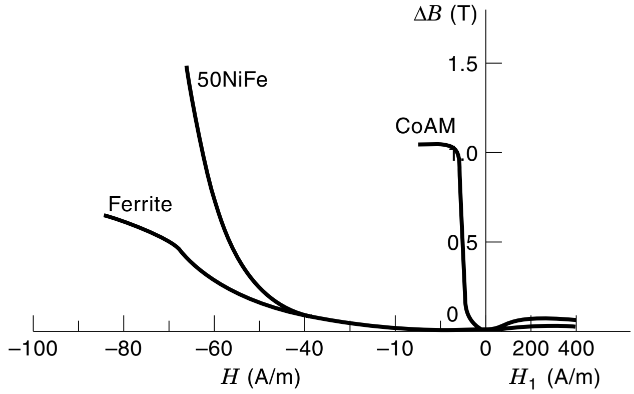

Figure 20. Controlled magnetization curves of Co-based amorphous (CoAM), anisotropic 50NiFe, and Mn–Zn ferrite (50 kHz) material.

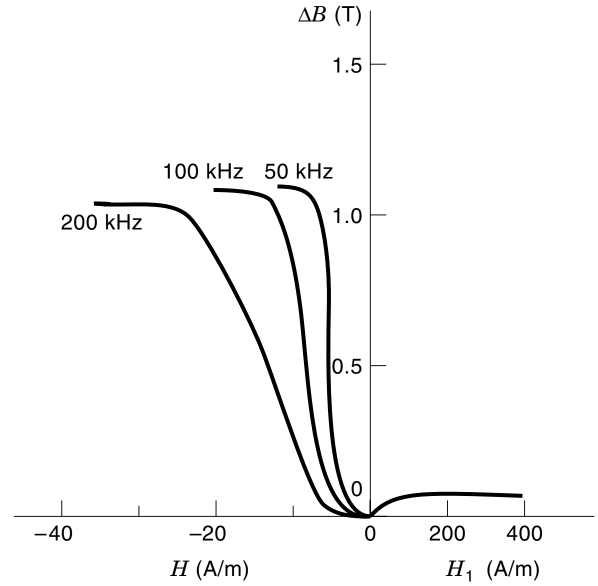

Figure 21. Frequency-dependent controlled magnetization curves of Co-based amorphous(CoAM) material, at under 50 kHz, 100 kHz, 200 kHz.

1. The controlling flux D_f of the magnetic amplifier is calculated by transformer output voltage time area;

$$D_f = (E_2 D_{on})/f \text{ (Wb)} \tag{15}$$

where E_2 is the transformer output voltage (V), D_{on} the maximum on-duty (s), and f the operating frequency (Hz).

2. Core size is selected based on controlling flux

$$D_f f_c A_w > (D_f I_0)/(K_f J) \text{(Wb mm}^2\text{)} \tag{16}$$

where f_c is the total flux (Wb), A_w is the window area of core (mm^2), I_0 is the nominal output current (A), K_f is the winding factor (in general, 0.4), and J is the average current density (A/mm^2).

3. The number of turns of winding, N, is

$$N > D_f/f_c \text{ (}N\text{ is an integer)} \tag{17}$$

4. Wire diameter d:

$$d = 2(I_0/\pi J)^{\frac{1}{2}} \text{ (mm}^2\text{)} \tag{18}$$

using thinner wire and litz wire is recommended as long as copper loss is permissible.

BIBLIOGRAPHY

1. Y. Murai et al., Describing function analysis of voltage-controlled capacitor motor with thyristors, *Elec. Eng. Jpn.,* **99**: 98–106, 1979.
2. H. W. Lord, *Magnetic Amplifiers: Electronics Engineers' Handbook,* 4th ed., New York: IEEE, 1997, pp. 17.75–17.82.
3. Y. Murai et al., Current peak limiting for a series resonant DC link power conversion using a saturable core, *Conf. Rec. 1991 Eur. Power Electron. Conf. (EPE),* Vol. 2, 1991, pp. 8–12.

4. N. Mohan, T. M. Undeland, and W. P. Robbins, *Power Electronics,* 2nd ed., New York: Wiley, 1995, pp. 69–76.
5. J. G. Gibson, *Non-linear Automatic Control,* New York: McGraw-Hill, 1963.
6. IEC Standard 404-1: Magnetic Materials, 1979.
7. G. L. Trigg (ed.), *Encyclopedia of Applied Physics,* Vol. 15, New York: VCH, 1996.
8. R. A. McCurie, *Ferromagnetic Materials,* London: Academic, 1994.
9. P. Robert, *Electrical and Magnetic Properties of Materials,* Norwood, MA: Artech House, 1988.
10. ASTM A598-69: Standard Test Method for Magnetic Properties of Magnetic Amplifier Cores, 1987.

YOSHIHIRO MURAI
T. SASAKI
Y. OKAZAKI
Gifu University

SCALAR MULTIPLICATION. See VECTORS.
SCANNERS. See DOCUMENT IMAGE PROCESSING; IMAGE SCANNERS.
SCANNERS, BARCODE. See MARK SCANNING EQUIPMENT.
SCANNERS FOR IMAGE PROCESSING. See IMAGE PROCESSING EQUIPMENT.
SCANNING. See IMAGE SCANNERS.